A Single-Phase Current Source Solar Inverter with Reduced-Size DC Link

Craig R. Bush Bingsen Wang
Student Member, IEEE Senior Member, IEEE
Arizona State University
P.O. Box 875706
Tempe, AZ 85287, USA
craig.bush@asu.edu; bingsen@asu.edu

***Abstract* -- This paper presents a new current source converter topology that is primarily intended for single-phase photovoltaic (PV) applications. In comparison against the existing PV inverter technology, the salient features of the proposed topology are: a) the low frequency (double of line frequency) ripple that is common to single-phase inverter has been eliminated; b) the absence of low frequency ripple enables significantly reduced-size passive components to achieve necessary stiffness; and c) improved maximum-power-point-tracking performance is readily achieved due to the tightened current ripple even with reduced-size passive components. This paper presents the proposed topology and its working principle backed up with numerical verifications.**

***Index Terms* — closed-loop control, current source inverter, photovoltaic, power conversion, pulse width modulation**

I. INTRODUCTION

The ever increasing demand for clean energy that is alternative to the conventional fossil-fuel based power generation has been one of the primary driving forces for the recent development of photovoltaic (PV) technologies, especially in the past decade. The majority of new installations of PV generation systems is grid interactive and enjoyed a 70%-increase of capacity worldwide in 2008 [*1*]. The power electronic converter is an indispensible subsystem that interfaces the PV modules with electric power systems.

As indicated by a rich body of literature records, various new topologies of PV inverters have been proposed and studied [*2*], [*3*]. Nonetheless, previous study suggests that the PV inverter still remains the weak link in PV power generation systems with regard to its reliability [*4*]. The lifetime of PV inverters is approximately 5-10 years as opposed to the 30-year lifetime of PV panels. The relatively short lifetime of inverters not only increases the effective operating cost, but also poses a significant stress on the environment in light of life cycle analysis, which contradicts one of the primary motivations of developing renewable energy generation, namely to relieve the stress to the environment imposed by the energy production processes.

The key issues related to PV inverters that negatively affect the reliability performance include the electrolytic capacitor, which commonly exists in PV inverters using the dominant topology of voltage source inverters (VSIs). The less frequently researched current source inverters (CSIs) could potentially eliminate the electrolytic capacitors while providing additional benefits as identified in [*5*]. It is worth noting that the current source inverter under consideration differs from the load commutated inverter (LCI) that is employed in high-power electric drives [*6*]. Three-phase CSI has been proposed for applications in PV generation systems [*5*]. However, for residential systems of the capacity below 10 kW peak power, the single-phase topology is predominant.

For single phase dc/ac inverter systems, with no regard to either VSI or CSI topology, the pulsating nature of the instantaneous power flow is in common as further detailed by the explanation in Section II. The pulsating power flow will manifest itself in the form of either dc-link current ripple or voltage ripple in a single-phase CSI or VSI, respectively. The low-frequency ripple on the dc-link will potentially have the following adverse consequences:

i. *Large-size passive components*
Although the modern semiconductor power devices such as insulated gate bipolar transistor (IGBT) offer the capability of switching at the high frequency of tens kHz, the specifications of some of the passive components in a design have to be based on the low frequency since the ripple current or voltage will be dominated by the low-frequency components. The resultant bulky design will not only be unappealing with regard to the associated cost ineffectiveness, but also present a considerable challenge to system design integration that is critical to achieve high reliability.

ii. *Degraded waveform quality*
The low frequency ripple on the dc link will be transferred to the undesired harmonics in the ac waveforms through the pulse width modulation process.

iii. *Suboptimal performance*
In PV generation system, the low-frequency ripple of the dc link voltage or current will negatively impact the performance of the maximum power point tracking (MPPT), which is almost a must in PV systems to maximize the utilization of the power generation asset. Furthermore, the system dynamic performance is degraded due to the large-size passive components.

The proposed topology is intended to address the above mentioned issues. The rest of the paper is organized as follows. The pulsating instantaneous power in single-phase

system and its impact to MPTT in PV generation systems are explained in Section II. The proposed topology is described in Section III and its operating principle is presented in Section IV. The modulation strategy is introduced in Section V followed by the discussion of control design in Section VI. The numerical simulation results presented in Section VII validate the proposed topology, modulation strategy and control algorithms. Section VIII concludes the paper with a summary.

II. Low Frequency Ripple in Single Phase Systems

In a single-phase system, if the grid voltage v and the injected current i are given by

$$v(t) = V\ \cos(\omega t);\ \ i(t) = I\ \cos(\omega t + \phi) \tag{1}$$

where V and I are the magnitudes of the grid voltage and the current supplied by the inverter, respectively;
ω is the angular frequency of the ac system;
ϕ is the phase angle difference between the voltage and the current, which is known as the power factor angle.
Then the instantaneous power flow p(t) is given by

$$\begin{aligned} p(t) &= v(t)i(t) \\ &= \underbrace{\frac{1}{2}VI\cos(\phi)}_{\text{constant term}} + \underbrace{\frac{1}{2}VI\cos(2\omega t + \phi)}_{\substack{\text{time-varying term} \\ \text{at twice line frequency}}} \end{aligned} \tag{2}$$

The low-frequency (relative to the high switching frequency at which modern power switches are capable to operate) ripple, as indicated by "time-varying term" in (2), will cause dc-link current ripple or voltage ripple in a single-phase CSI or VSI, respectively. The oscillating current or voltage will degrade the performance of MPPT in PV power generation system. Fig. 1 illustrates a typical i-v characteristic of a PV panel on the i_{pv}-v_{pv} plane. A power curve is overlaid on top of the i-v curve in the p_{pv}-v_{pv} plane. As the power output from the PV panel reaches the maximum P_{max} on the power curve, the maximum power point on the i-v curve correspond to the point 'P' labeled in Fig. 1. The terminal voltage and current V_{max} and I_{max} at which the PV panel delivers the maximum power are not label on the axes i_{pv} and v_{pv} for avoidance of cluttering the figure. It is evident that the output power will be typically below P_{max} if the terminal voltage varies around V_{max} except discrete operating points. In a similar situation, the suboptimal operation will result if the terminal current varies in the vicinity of I_{max}.

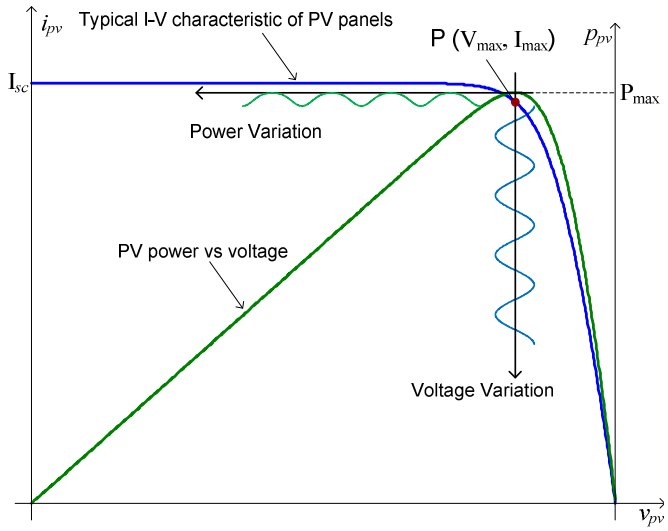

Fig. 1 Illustration of the low-frequency effect on maximum power point tracking in a PV system.

III. Proposed Topology

The power circuit of the proposed topology is illustrated by the schematic in Fig. 2. A CSI bridge consists of six voltage bidirectional switches (VBS): three upper switches S_{au}, S_{bu}, S_{cu} and three lower switches S_{al} , S_{bl}, S_{cl}. The VBS in the schematic is depicted as a series connection of an IGBT and a diode, it is possible to replace it with a single-device that is capable of blocking bipolar voltages. For instance, reverse blocking IGBT devices can be utilized.

On the dc side of the converter, an inductor L_{dc} connects the PV panel. In a typical single-phase inverter, the dc link inductor has to be sized significantly large to maintain the double-frequency ripple current, which is resulted from the pulsating instantaneous power flow, at a sufficiently low level for proper operation of the converter. However, the dc link inductor in this proposed topology can be sized according to the switching frequency ripple components. Hence, the size of the inductor can be significantly smaller than the conventional single phase inverter.

On the ac side of the converter, phase-legs *a* and *c* of the bridge are connected to the grid voltage v_g through an LC filter that is composed of L_f and C_f. The phase-leg *b* of the converter bridge is connected to the grid through the capacitor C_b. The voltage across the capacitor C_b will be only subject to the current flowing through phase-leg *b*, namely i_b. With proper control of the current i_b, it is possible to achieve constant instantaneous power flow across the bridge, which will be further explained in Section IV.

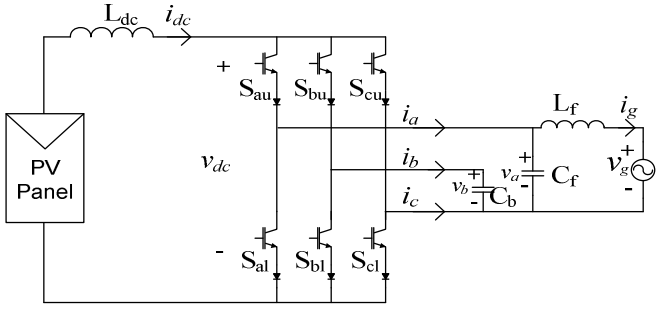

Fig. 2 Schematic of the proposed single phase PV inverter topology.

IV. OPERATING PRINCIPLE

The key to the operation of the proposed topology lies in the control of the converter bridge such that the *instantaneous power* transfer across the switching bridge is maintained *constant*. For the determination of the appropriate phase *b* current i_b the concept of space vector is utilized [7].

The voltage space vector at the ac terminals of the converter is defined as

$$\underline{v} = \frac{2}{3}(v_a + \alpha v_b + \alpha^2 v_c) \tag{3}$$

where $\alpha = e^{j2\pi/3}$.
The three-phase voltages are assumed

$$\begin{aligned} v_a &= V_a \cos(\omega t) \\ v_b &= V_b \cos(\omega t + \phi_{vb}) \\ v_c &= 0 \end{aligned} \tag{4}$$

with the voltage magnitude V_b of phase *b* and its phase angle ϕ_{vb} to be determined. Substitution of (4) into (3) yields

$$\underline{v} = \frac{1}{3}\left(V_a + \alpha V_b e^{j\phi_{vb}}\right)e^{j\omega t} + \frac{1}{3}\left(V_a + \alpha V_b e^{-j\phi_{vb}}\right)e^{-j\omega t} \tag{5}$$

The space vectors $\underline{v}_p$ and $\underline{v}_n$ that correspond to the positive and negative sequence components are identified from (5) as

$$\begin{aligned} \underline{v}_p &= \frac{1}{3}\left(V_a + \alpha V_b e^{j\phi_{vb}}\right)e^{j\omega t} \\ \underline{v}_n &= \frac{1}{3}\left(V_a + \alpha V_b e^{-j\phi_{vb}}\right)e^{-j\omega t} \end{aligned} \tag{6}$$

In a similar manner, the current space vector at the ac terminals of the converter is

$$\underline{i} = \frac{2}{3}(i_a + \alpha i_b + \alpha^2 i_c) \tag{7}$$

The three-phase currents are given by

$$\begin{aligned} i_a &= I_a \cos(\omega t + \phi) \\ i_b &= I_b \cos(\omega t + \phi_{ib}) \\ i_c &= -i_a - i_c \end{aligned} \tag{8}$$

where ϕ is the power factor angle, which is zero for unity power factor operation. The magnitude I_b and the phase angle ϕ_{ib} of phase *b* current are to be determined.
Substitution of (8) into (7) leads to

$$\begin{aligned} \underline{i} = &\frac{1}{\sqrt{3}}\left[I_a e^{j\left(\phi+\frac{\pi}{6}\right)} + jI_b e^{j\phi_{ib}}\right]e^{j\omega t} + \\ &\frac{1}{\sqrt{3}}\left[I_a e^{j\left(-\phi+\frac{\pi}{6}\right)} + jI_b e^{-j\phi_{ib}}\right]e^{-j\omega t} \end{aligned} \tag{9}$$

The current space vectors $\underline{i}_p$ and $\underline{i}_n$ that correspond to the positive and negative sequence components are defined accordingly as

$$\begin{aligned} \underline{i}_p &= \frac{1}{\sqrt{3}}\left[I_a e^{j\left(\phi+\frac{\pi}{6}\right)} + jI_b e^{j\phi_{ib}}\right]e^{j\omega t} \\ \underline{i}_n &= \frac{1}{\sqrt{3}}\left[I_a e^{j\left(-\phi+\frac{\pi}{6}\right)} + jI_b e^{-j\phi_{ib}}\right]e^{-j\omega t} \end{aligned} \tag{10}$$

The instantaneous power flow across the converter can be expressed in terms of the defined voltage and current space vectors $\underline{v}$ and $\underline{i}$.

$$\begin{aligned} p(t) &= \frac{3}{2}Re\left(\underline{v}\,\underline{i}^*\right) \\ &= \underbrace{\frac{3}{2}Re\left(\underline{v}_p\underline{i}_p^* + \underline{v}_n\underline{i}_n^*\right)}_{p_1(t)} + \underbrace{\frac{3}{2}Re\left(\underline{v}_p\underline{i}_n^* + \underline{v}_n\underline{i}_p^*\right)}_{p_2(t)} \end{aligned} \tag{11}$$

where $Re(\cdot)$ denotes the real component of a complex quantity and '*' denotes the conjugate of a complex variable. With reference to (6) and (10), the two terms p_1(t) and p_2(t) in (11) can be determined after algebraic manipulation to be

$$\begin{aligned} p_1(t) &= \frac{1}{2}V_a I_a \cos(\phi) \\ p_2(t) &= \frac{1}{2}[V_a I_a \cos(2\omega t + \phi)] \\ &\quad + V_b I_b \cos(2\omega t + \phi_{vb} + C_b V_a) \end{aligned} \tag{12}$$

In order for $p(t)$ to be constant, it requires $p_2(t)$ to be constant (i.e. zero) since $p_1(t)$ is constant. Based on the relation between the voltage across and the current through a capacitor, it follows that

$$I_b = \omega C_b V_b; \qquad \phi_{ib} = \phi_{vb} + \frac{\pi}{2} \tag{13}$$

Substituting (13) into the second equation of (12) and solving $p_2(t) = 0$ for I_b and ϕ_{ib} results in

$$I_b = \sqrt{\omega C_b V_a I_a} \quad ; \quad \phi_{ib} = \tfrac{1}{2}(\phi - \tfrac{\pi}{2}) \tag{14}$$

Equation (14) describes the critical condition for maintaining the instantaneous power flow across the converter bridge to be constant.

V. MODULATION SCHEME

The primary functionality of the modulator is to determine the switching sequence of for the power switches so that the desired output currents can be synthesized. The design of the modulator involves a two-step process: first the continuous modulation functions (or duty ratios) of the switches are determined and then the discontinuous switching functions are determined based on these modulation functions.

A. Modulation Functions

The modulation functions for the six switches S_{au}, S_{bu}, S_{cu}, S_{al}, S_{bl}, and S_{cl} of the bridge in Fig. 2 are denoted as m_{au}, m_{bu}, m_{cu}, m_{al}, m_{bl}, and m_{cl}, respectively. The topological constraints of the CSI bridge requires one and only one of the upper switches $\{S_{au}, S_{bu}, S_{cu}\}$ together with one and only one of the lower switches $\{S_{al}, S_{bl}$, and $S_{cl}\}$ be

turned on at any instant of time so that the open-circuit of the dc link and short-circuit of ac terminals can be simultaneously avoided. This requirement can be described by the mathematical constraints on the modulation functions, i.e.

$$\begin{aligned} m_{au} + m_{bu} + m_{cu} &= 1 \\ m_{al} + m_{bl} + m_{cl} &= 1 \\ 0 \le m_{au}, m_{bu}, m_{cu}, m_{al}, m_{bl}, m_{cl} &\le 1 \end{aligned} \tag{15}$$

Unlike the determination of the modulation functions in a three-phase balanced system, it is not a straightforward exercise when determining the modulation functions subject to the constraints of (15) given the desired fundamental components of i_a, i_b, and i_c in Fig. 2. The problem is approached by decomposing the modulation functions into the positive- and negative-sequence components.

$$\begin{aligned} m_{au} &= m_{aup} + m_{aun} & m_{al} &= m_{alp} + m_{aln} \\ m_{bu} &= m_{bup} + m_{bun} & m_{bl} &= m_{blp} + m_{bln} \\ m_{cu} &= m_{cup} + m_{cun} & m_{cl} &= m_{clp} + m_{cln} \end{aligned} \tag{16}$$

where m_{aup}, m_{bup}, m_{cup}, m_{alp}, m_{blp}, and m_{clp} are the positive sequence components while m_{aun}, m_{bun}, m_{cun}, m_{aln}, m_{bln}, and m_{cln} being the negative sequence components. These positive and negative sequence modulation functions are separately derived from the corresponding space vectors as explained below.

With the aid of (14), the positive and negative sequences of the converter current vectors in (10) can be rewritten as the following

$$\begin{aligned} \underline{i}_p &= \frac{1}{\sqrt{3}}\left[I_a e^{j\left(\phi+\frac{\pi}{6}\right)} + j\sqrt{\omega C_b V_a I_a}\, e^{j\left(\frac{\phi}{2}+\frac{\pi}{4}\right)}\right] e^{j\omega t} \\ \underline{i}_n &= \frac{1}{\sqrt{3}}\left[I_a e^{j(-\phi+\frac{\pi}{6})} + j\sqrt{\omega C_b V_a I_a}\, e^{-j(\frac{\phi}{2}-\frac{3\pi}{4})}\right] e^{-j\omega t} \end{aligned} \tag{17}$$

The corresponding positive and negative sequence components of the modulation space vectors are obtained by normalizing the current space vectors to the dc link current

$$\underline{m}_p = \frac{\underline{i}_p}{I_{dc}};\ \underline{m}_n = \frac{\underline{i}_n}{I_{dc}} \tag{18}$$

For the positive sequence, the modulation functions are

$$\begin{aligned} m_{aup} &= m_{ap}\Phi(m_{ap}) + m_{p0} \\ m_{alp} &= -m_{ap}\Phi(-m_{ap}) + m_{p0} \\ m_{bup} &= m_{bp}\Phi(m_{bp}) + m_{p0} \\ m_{blp} &= -m_{bp}\Phi(-m_{bp}) + m_{p0} \\ m_{cup} &= m_{cp}\Phi(m_{cp}) + m_{p0} \\ m_{clp} &= -m_{cp}\Phi(-m_{cp}) + m_{p0} \end{aligned} \tag{19}$$

where the modulation functions m_{ap}, m_{bp}, and m_{cp} are the *abc* components of the rotating vector $\underline{m}_p$ and they are calculated according to the following transformation

$m_{ap} = Re(\underline{m}_p);\ m_{bp} = Re(\alpha^2\,\underline{m}_p);\ m_{cp} = Re(\alpha\,\underline{m}_p)$

$\Phi(x)$ is a step function defined as

$$\Phi(x) = \begin{cases} 1 & \text{if } x > 0 \\ 0 & \text{otherwise} \end{cases}$$

and the common mode component m_{p0} for the positive sequence is

$$m_{p0} = \frac{\frac{|\underline{m}_p|}{|\underline{m}_p| + |\underline{m}_n|} - \max(m_{ap}, m_{bp}, m_{cp})}{3}.$$

In a similar manner, the negative-sequence components of the modulation functions are

$$\begin{aligned} m_{aun} &= m_{an}\Phi(m_{an}) + m_{n0} \\ m_{aln} &= -m_{an}\Phi(-m_{an}) + m_{n0} \\ m_{bun} &= m_{bn}\Phi(m_{bn}) + m_{n0} \\ m_{bln} &= -m_{bn}\Phi(-m_{bn}) + m_{n0} \\ m_{cun} &= m_{cn}\Phi(m_{cn}) + m_{n0} \\ m_{cln} &= -m_{cn}\Phi(-m_{cn}) + m_{n0} \end{aligned} \tag{20}$$

where the modulation functions m_{an}, m_{bn}, and m_{cn} are the *abc* components of the rotating vector $\underline{m}_n$ and they are

$m_{an} = Re(\underline{m}_n);\ m_{bn} = Re(\alpha^2\underline{m}_n);\ m_{cn} = Re(\alpha\,\underline{m}_n)$

the common mode component m_{n0} for the negative sequence is

$$m_{n0} = \frac{\frac{|\underline{m}_n|}{|\underline{m}_p| + |\underline{m}_n|} - \max(m_{an}, m_{bn}, m_{cn})}{3}.$$

A typical set of waveforms for the modulation functions m_{au}, m_{bu}, m_{cu} of the upper switches and the modulation functions m_{al}, m_{bl}, m_{cl} of the lower switches are obtained by following the described modulation process and they plotted for one fundamental period as shown in Fig. 3.

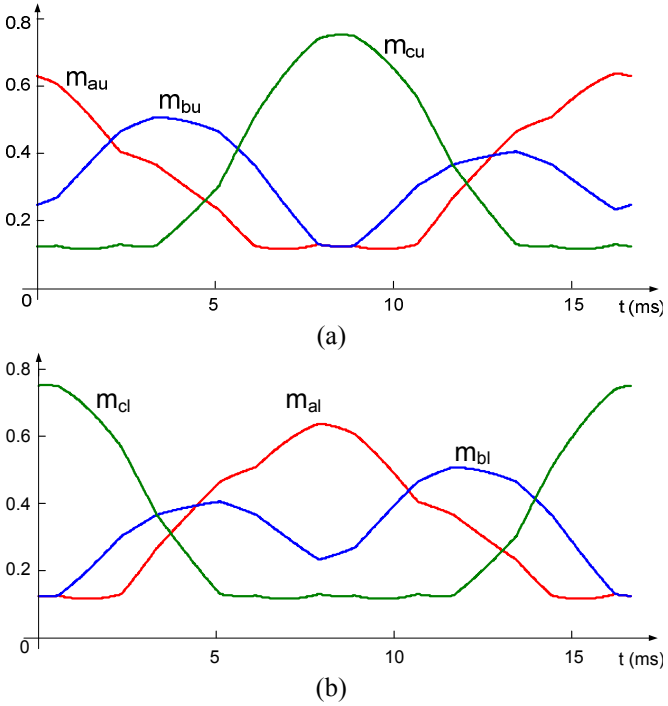

Fig. 3 Typical waveforms of (a) the modulation functions m_{au}, m_{bu}, and m_{cu} (b) the modulation functions m_{al}, m_{bl}, and m_{cl} in one fundamental period.

B. Switching Functions

A carrier based PWM method is adopted to generate the switching functions. Let h_{au}, h_{bu}, h_{cp} be switching functions of the upper switches in Fig. 2. These switching functions h_{au}, h_{bu} can be generated by comparison of modulation functions against a triangular carrier signal. Then the switching function h_{cu} is derived as $h_{cu} = 1 - h_{au} - h_{bu}$. The modulation process is pictorially illustrated in Fig. 4. The generated switching functions will be used as logic signals to turn-on and -off the physical semiconductor switches of the CSI bridge.

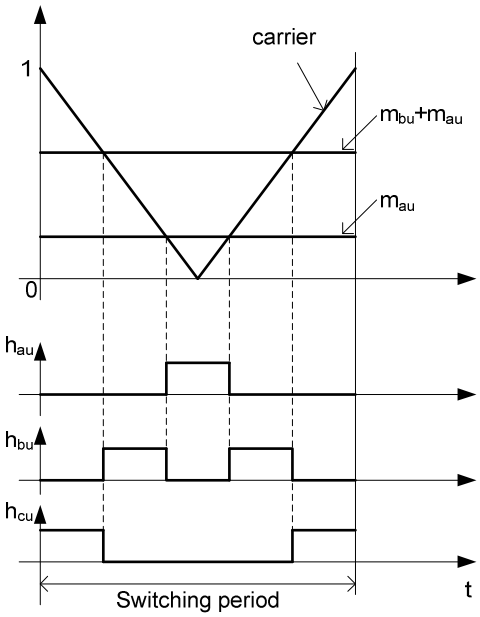

Fig. 4 Illustration of generating switching functions based on a carrier-based modulation scheme.

VI. CONTROL DESIGN

The control objectives of include simultaneous regulation of the dc link current and the ac current that is fed into the power grid. The controller structure is illustrated in Fig. 5. The dc link current i_{dc} is sensed and compared against the reference i_{dc}^*. The output of the dc current regulator forms the reference of the q-axis component of the grid current, i_{gq}^*, which determines the active power flow. The reference of the d-axis component of the grid current, i_{gd}^*, is calculated from the reactive power command Q^* and the measured grid voltage amplitude. The ac current regulator that will generate the references for the converter output current i_a^*, which will further be used as the command for the modulator. The grid voltage magnitude and the phase angle are measured by a phase-locked loop (PLL) [*8*]. The grid phase angle θ_g is used in the single phase ac to dq transformation and its inverse transform. One method of generating dq coordinates based on Hilbert transform in a single phase system is presented in [*9*]. This paper does not utilize the Hilbert transform to generate the orthogonal signal (on β-axis). Instead an all pass filter is used method developed in [*10*] is utilized. This method passes the original signal (on α-axis) into the following transfer function

$$H(s) = \frac{1 - T_1 s}{1 + T_1 s} \tag{21}$$

where $T_1 = 1/\omega_1$ and ω_1 is the fundamental angular frequency. This generated the desired orthogonal signal.

The ac current regulator features a dual-loop structure [*11*] as illustrated in Fig. 6. The gain R_a determines the bandwidth of inner voltage loop. A state feedback decoupling has been used employed for the inner voltage control. For the outer current loop control, the measured grid voltage is utilized in the disturbance rejection. A proportional and integral regulator is utilized to regulate the current injected into the grid. The controller parameters K_i, K_v are calculated to maintain the desired bandwidths. It is worth noting that the PI regulator in dq reference frame will result in zero steady state error in terms of both magnitude and phase angle.

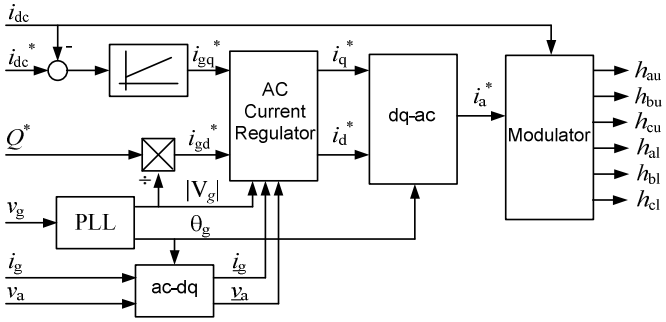

Fig. 5 Block diagram of the overall control structure.

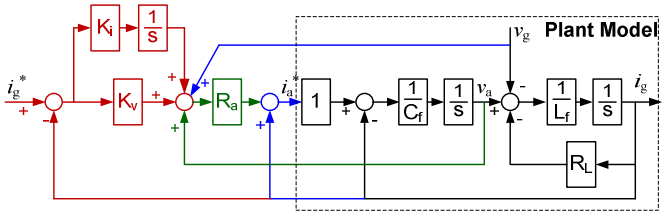

Fig. 6 Block diagram ac current regulator.

VII. SIMULATION RESULTS

A detailed model of power circuit and the proposed control structure has been implemented with Saber™. The simulation results of the salient waveforms are illustrated in the following figures. The grid voltage v_g and the current i_g shown in Fig. 7 are in phase under the unity-power-factor operating condition. The filter capacitor voltage and the converter output current are shown in Fig. 8 Simulated waveforms of the filter capacitor voltage v_a and the converter output current i_a.Fig. 8. The dc link voltage v_{dc} and its spectrum are shown in Fig. 9. From the spectrum of dc link voltage it is evident the double frequency ripple component has been minimized, which will allow for reduced size of the dc link inductor.

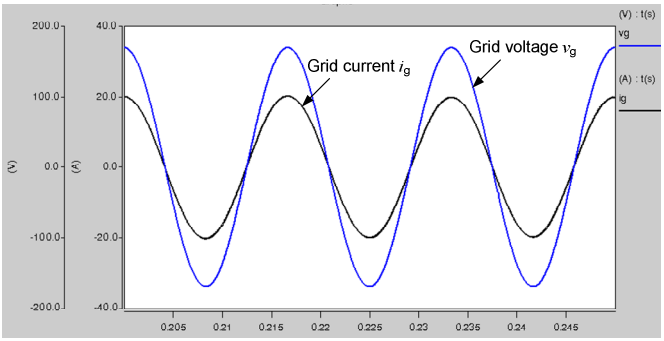

Fig. 7 Simulated waveforms of the grid voltage v_g and current i_g.

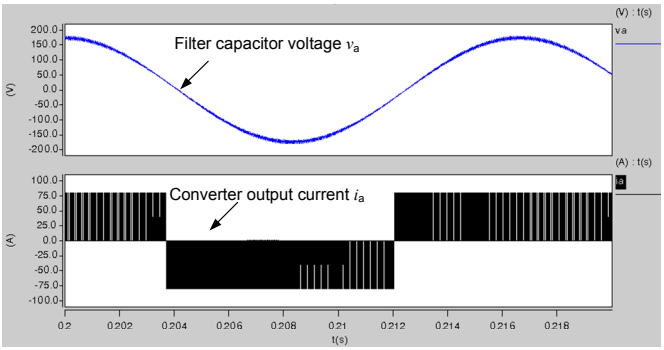

Fig. 8 Simulated waveforms of the filter capacitor voltage v_a and the converter output current i_a.

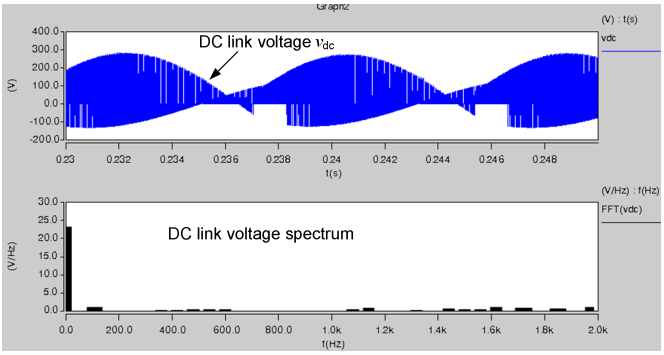

Fig. 9 Simulated waveform of the dc link voltage v_{dc} and its spectrum.

VIII. CONCLUSIONS

A new PV inverter topology has been presented to deal with the low frequency ripple that commonly exists in single-phase systems. The modulation and control algorithm have been proposed. It is worth noting the modulation approach developed for the single-phase application may be extended and applied to three-phase CSI system that runs under unbalanced operating conditions. The modulation and control methods have been verified by the numerical simulation results obtained from a detailed Saber™ model. A laboratory prototype is being constructed and the detailed experimental results will be reported in the future publications.

REFERENCES

[1] "Renewables Global Status Report," www.ren21.net, 2009.

[2] L. Wu and J. Liu, "A single-state three-phase grid connected photovoltaic system with modified MPTT method and reactive power compensation," *IEEE Transactions on Energy Conversion*, vol. 22, no. 4, pp. 881-886, 2007.

[3] S. A. Daniel, "A novel hybrid isolated generating system based on PV fed inverter-assisted wind-driven induction generators," *IEEE Transactions on Energy Conversion*, vol. 19, no. 2, pp. 416-422, 2004.

[4] R. Margolis, "A review of pv inverter technology cost and performance projections," National Renewable Energy Laboratory, NREL/SR 620-38771, 2006.

[5] Y. Chen, K. Smedley, and J. Brouwer, "A cost-effective three-phase grid-connected inverter with maximum power point tracking," in *Record of IEEE Industry Applications Society Annual Meeting*, Tampa, Florida, 2006, pp. 995-1000.

[6] B. Wang and J. J. Cathey, "DSP-controlled, space-vector PWM, current source converter for sitcom application," *Electric Power Systems Research*, vol. 67, no. 2, pp. 123-131, 2003.

[7] D. W. Novotny and T. A. Lipo, *Vector Control and Dyanmics of AC Drives*. New York: Oxford University Press, 1996.

[8] S. Chung, "A phase tracking system for three phase utility interface inverters," *IEEE Transactions on Power Electronics*, vol. 15, no. 2, pp. 431-438, 2000.

[9] M. Saito and N. Matsui, "A single to three-phase matrix converter for a vector-controlled induction motor," in *Record of IEEE Industry Applications Society Annual Meeting*, Edmonton, Canada, 2008, pp. 1-6.

[10] M. Haque and T. Ise, "Implementation of single-phase pq theory," in *Proceedings of Power Conversion Conference*, Osaka, Japan, 2002, pp. 761-765.

[11] M. Ryan, W. Brumsickle, and R. Lorenz, "Control topology options for single-phase ups inverters," *IEEE Transactions on Industry Applications*, vol. 22, no. 2, pp. 493-501, 1997.